東北大学機関リポジトリ
TOUR
Tohoku University Repository

東北大学

Large anisotropy in conductivity of Ti2O3\nfilms

	K. Yoshimatsu, H.Kurokawa, K.Horiba, H. Kumigashira, A.Ohtomo
journal or publication title	APL Materials
volume	6
number	101101
page range	1-8
year	2018-10-01
URL	http://hdl.handle.net/10097/00125546

doi: 10.1063/1.5050823

Large anisotropy in conductivity of Ti$_2$O$_3$ films

K. Yoshimatsu (iD), H. Kurokawa, K. Horiba, H. Kumigashira, and A. Ohtomo (iD)

View Online   Export Citation   CrossMark

ARTICLES YOU MAY BE INTERESTED IN

Band alignment at β-(Al$_x$Ga$_{1-x}$)$_2$O$_3$/β-Ga$_2$O$_3$ (100) interface fabricated by pulsed-laser deposition
Applied Physics Letters 112, 232103 (2018); https://doi.org/10.1063/1.5027005

Perspective: Emergent topologies in oxide superlattices
APL Materials 6, 100901 (2018); https://doi.org/10.1063/1.5046100

High-throughput screening of perovskite oxynitride and oxide materials for visible-light photocatalysis
APL Materials 6, 101103 (2018); https://doi.org/10.1063/1.5041784

Large anisotropy in conductivity of Ti$_2$O$_3$ films

K. Yoshimatsu,[1,a] H. Kurokawa,[1] K. Horiba,[2,3] H. Kumigashira,[2,3] and A. Ohtomo[1,3]

[1]*Department of Chemical Science and Engineering, Tokyo Institute of Technology, 2-12-1 Ookayama, Meguro-ku, Tokyo 152-8552, Japan*
[2]*Photon Factory, Institute of Materials Structure Science, High Energy Accelerator Research Organization (KEK), 1-1 Oho, Tsukuba, Ibaraki 305-0801, Japan*
[3]*Materials Research Center for Element Strategy (MCES), Tokyo Institute of Technology, 4259 Nagatsuta-cho, Midori-ku, Yokohama 226-8503, Japan*

We investigated electronic properties of Ti$_2$O$_3$ films with film thickness of ~150 nm. The temperature dependence of resistivity indicated characteristic phase transitions. The insulator-to-metal transition (IMT) temperature (T_{IMT}) deviated from bulk T_{IMT} of ~450 K. The higher and lower T_{IMT}s of 450–600 K and 200–300 K were found in *a*- and *c*-axes oriented films, respectively. In addition, the large anisotropy in conductivity parallel and perpendicular to the *c*-axis direction was observed in the insulating phase, which was attributed to large difference in Hall mobility. The higher T_{IMT} far above room temperature and the large difference in resistivity across the IMT were promising characteristics for application of Ti$_2$O$_3$ films in Mottronics. © *2018 Author(s). All article content, except where otherwise noted, is licensed under a Creative Commons Attribution (CC BY) license (http://creativecommons.org/licenses/by/4.0/).* https://doi.org/10.1063/1.5050823

Titanium dioxide (TiO$_2$) exhibits multi-functionality such as photocatalyst under UV light[1,2] and transparent conductivity of Nb-doped films.[3] The reduction of TiO$_2$ also leads to electric conductivity without the substitutional doping. The reduced titanates (TiO$_x$, $x < 2$) have been investigated in terms of a variety of crystalline polymorphs and electronic phase transitions. For example, superconductivity with maximum transition temperature (T_C) of 2.3 K appears in TiO and T_C is strongly affected by oxygen non-stoichiometry and/or the number of defects.[4,5] Moreover, Magnéli phase Ti$_n$O$_{2n-1}$ ($n \geq 4$) is known to show metal-insulator transition at ~150 K.[6–8] Large electron-phonon interaction is responsible for these characteristic physical properties.[9,10] Recently, reduced titanates in a thin-film form were paid much attention owing to peculiar superconducting phases observed in TiO, Rh$_2$O$_3$-type Ti$_2$O$_3$, γ-Ti$_3$O$_5$, and Ti$_4$O$_7$.[11–13] Zhang *et al.* reported on enhanced superconductivity in TiO with T_C up to 7.4 K,[11] which was higher by three times than maximum T_C of bulk. In the other reduced titanates, superconductivity appeared only in the thin film form with T_Cs of 8.0, 7.1, and 3.0 K for Rh$_2$O$_3$-type Ti$_2$O$_3$, γ-Ti$_3$O$_5$, and Ti$_4$O$_7$, respectively.[12,13] The emergence of intriguing electronic properties of the thin films motivates us to further investigate other reduced titanates in the thin-film form.

Corundum-type Ti$_2$O$_3$ is also a member of reduced titanates which shows insulator-to-metal transition (IMT) around 450 K in bulk.[14–19] The higher IMT temperature (T_{IMT}) is similar to vanadium dioxide (VO$_2$ with $T_{IMT} \sim 340$ K in bulk[20–28]) with the identical d^1 configuration. VO$_2$ is one of the most popular transition-metal oxides regarded as a Mottronics material. In the Mottronics material, the higher T_{IMT} above room temperature and larger resistivity change across the IMT are preferable. The former characteristic is important for large integration of devices operable under much exhaust heat. The latter characteristic is favorable for making clear on/off states. Although Ti$_2$O$_3$ is superior to VO$_2$ in the former characteristic, difficulty in the epitaxial growth of reduced titanate films hampers

---

[a]Author to whom correspondence should be addressed: k-yoshi@apc.titech.ac.jp

investigation of Ti_2O_3 films as the Mottronics material. However, recent advancement in pulsed-laser deposition (PLD) using TiO_x targets enabled us to obtain various reduced titanate films,[11–13,29] and thus exploring the electronic functionality of Ti_2O_3 films was anticipated.

In this Letter, we report on the structural and electronic properties of Ti_2O_3 films. The *a*- and *c*-axes oriented high-quality Ti_2O_3 films were grown on *a*- and *c*-planes of isostructural α-Al_2O_3 substrates, respectively. The formation of the corundum-type Ti_2O_3 films was also confirmed from x-ray absorption and photoemission spectroscopy (PES). The temperature dependence of in-plane resistivity revealed the large difference in T_{IMT} between *a*- and *c*-axes oriented Ti_2O_3 films. The stability of the insulating phase was enhanced for the *a*-axis oriented films. Moreover, the higher (lower) resistivity in the insulating phase was found for *a*-axis oriented Ti_2O_3 films along the direction of current $I//c$ ($I \perp c$). We observed clear IMT at 450–600 K with a resistivity drop by three orders of magnitude along $I//c$. The anisotropy in conductivity was attributed to anisotropy in mobility revealed from the temperature dependence of Hall-effect measurements. These characteristics could be explained by the film orientation and current path with respect to the Ti–Ti pairs.

Ti_2O_3 films with a thickness of ~150 nm were grown on α-Al_2O_3 (0001) and (11$\bar{2}$0) substrates by using PLD equipped with a KrF excimer laser (20 Hz, 1 J/cm^2). A polycrystalline Ti_2O_3 target, placed 5 cm away from the substrate surface, was prepared by a conventional solid-state reaction method. Ti (3N purity) and TiO_2 (4N purity) powders with a molar ratio of 1:3 were mixed and pressed into a pellet. It was sintered at 1100 °C for 12 h in vacuum to obtain the target with a nominal composition of Ti_2O_3. Prior to the film growth, α-Al_2O_3 substrates were annealed at 1100 °C for 9 h in air to obtain the step-and-terrace surfaces. Growth temperature and Ar (6N purity) partial pressure in the PLD chamber were set 1000 °C and 1×10^{-3} Torr, respectively. The higher growth temperature of 1000 °C was essential to obtain single oriented Ti_2O_3 films on *a*-plane α-Al_2O_3 substrates. In addition, the use of Ar gas repelled residual oxygen in the PLD chamber whose base pressure is ~1×10^{-8} Torr. The usefulness of Ar gas for growth of low-valence oxide films was also reported on perovskite molybdenites.[30] After the growth, Ti_2O_3 films were quenched to room temperature while keeping the chamber pressure constant. The detailed thin-film growth of various reduced titanates is reported elsewhere.[13,29]

Crystal structures of the films were characterized by x-ray diffraction (XRD) with Cu Kα_1 radiation (λ = 1.5406 Å) (Rigaku, SmartLab). Thickness of the Ti_2O_3 films was measured by using a stylus-type profiler (KLA Tencor, Alpha-Step D-500). The experimental errors of film thickness were less than 10 nm. Surface morphology was observed by atomic force microscopy (AFM). Ti (30 nm)/Au (100 nm) electrodes were deposited on the films for the electrical measurements. In addition, Al wires were driven into the films in order to avoid effects of the surface oxidation layers. Temperature dependence of the resistivity was measured in a standard four-probe method using the physical properties measurement system (Quantum Design, PPMS) in a low temperature range ($T \leq 400$ K) and ResiTest 8300 (Toyo Corporation) in a high temperature range (300 K $\leq T \leq$ 650 K). Temperature dependence of Hall-effect measurements was carried out in a Hall-bar geometry using PPMS.

PES and x-ray absorption spectroscopy (XAS) were performed at the undulator beamline of BL2A at Photon Factory, KEK. Before PES and XAS measurements, the surface of Ti_2O_3 films was treated by Ar-bombardment in order to remove surface oxidation layers (their thickness was expected to be a few nm from PES measurements). PES spectra were recorded using an electron energy analyzer (SES-2002, VG Scienta). The total energy resolution was set to about 200 meV at $h\nu$ = 800 eV. The Fermi level was referred to that of Au electrically in contact with the sample surface. XAS spectra were taken in the total electron yield mode. All the spectra were taken at room temperature.

Figure 1(a) shows wide-range out-of-plane XRD patterns with 2θ from 10° to 100° of Ti_2O_3 films on α-Al_2O_3 (0001) substrates. Film peaks were detected at $2\theta \sim$ 39° and 84°, which were assigned as the Ti_2O_3 0006 and 000$\underline{12}$ reflections, respectively. No other film peaks were found in the wide-range XRD patterns. The AFM image [inset of Fig. 1(a)] reflected a trace of the spiral growth.[31] These results confirm growth of *c*-axis oriented Ti_2O_3 films on α-Al_2O_3 (0001) substrates. Moreover, the films were confirmed to be of high quality by the sharp ω-scan rocking curve of the Ti_2O_3 0006 reflection with a full width at half maximum (FWHM) of ~0.05° [inset of Fig. 1(a)].
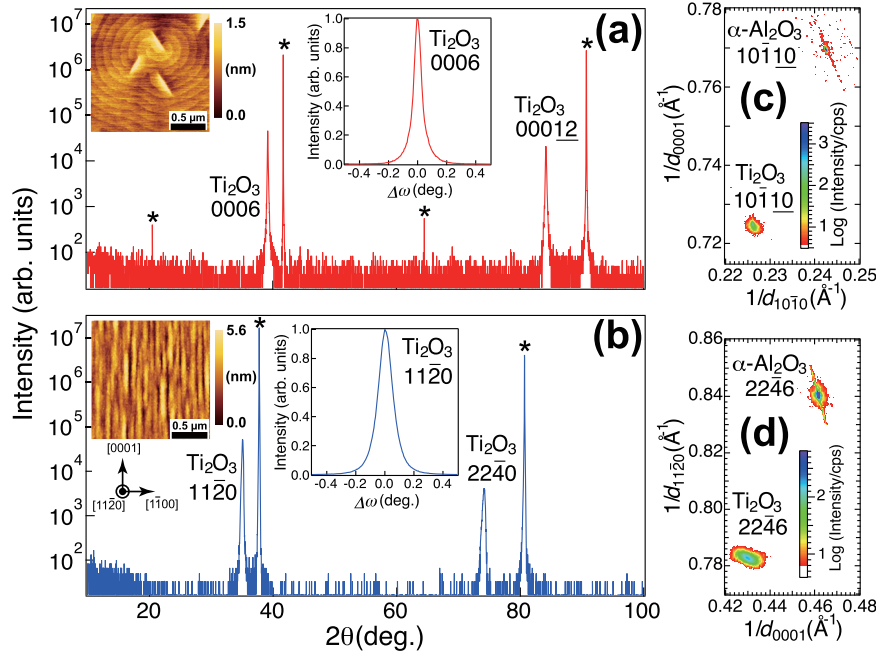
FIG. 1. Structural properties of Ti_2O_3 films. Wide-range out-of-plane XRD patterns with 2θ from $10°$ to $100°$ of (a) c- and (b) a-axis oriented Ti_2O_3 films using Cu $K\alpha_1$ x-ray ($\lambda = 1.5406$ Å). The asterisks ($*$) indicate reflections from the substrates. The insets show AFM images of the films (left) and ω-scan rocking curve profiles of Ti_2O_3 0006 in (a) and $11\bar{2}0$ reflections in (b) (right). Reciprocal space map around (c) α-Al_2O_3 $10\bar{1}10$ reflections of c-axis oriented Ti_2O_3 films and (d) α-Al_2O_3 $22\bar{4}6$ reflections of a-axis oriented Ti_2O_3 films.

The a-axis oriented Ti_2O_3 films were grown on α-Al_2O_3 ($11\bar{2}0$) substrates. The wide-range out-of-plane XRD pattern with 2θ from $10°$ to $100°$ [Fig. 1(b)] clearly indicated the Ti_2O_3 $11\bar{2}0$ and $22\bar{4}0$ reflections detected at $2\theta \sim 35°$ and $74°$, respectively. No other film peaks were found in the XRD pattern. The surface morphology was dissimilar to that of the c-axis oriented film. The small grains elongated along the [0001] direction were found in the AFM image [inset of Fig. 1(b)], suggesting the columnarlike growth. The FWHM of the ω-scan rocking curve of the Ti_2O_3 $11\bar{2}0$ reflection was $\sim 0.1°$ [inset of Fig. 1(b)]. The crystallinity of the a-axis oriented film was also high but slightly worse than that of the c-axis oriented one. These results indicate that high-quality a- and c-axes oriented Ti_2O_3 films were obtained on different planes of α-Al_2O_3 substrates.

In order to further investigate the crystal structures, we measured reciprocal space maps (RSMs). Figure 1(c) shows the RSM around α-Al_2O_3 $10\bar{1}10$ reflection of the c-axis oriented Ti_2O_3 film. The Ti_2O_3 $10\bar{1}10$ reflection was detected at $(1/d_{10\bar{1}0}, 1/d_{0001}) = (0.226, 0.725)$, corresponding to the lattice constants of $a = 5.104$ Å and $c = 13.80$ Å. The lattice constants of the a-axis oriented film were also estimated from the RSM. Figure 1(d) shows the RSM around α-Al_2O_3 $22\bar{4}6$ reflection of the a-axis oriented Ti_2O_3 film. The Ti_2O_3 $22\bar{4}6$ reflection was detected at $(1/d_{0001}, 1/d_{11\bar{2}0}) = (0.430, 0.783)$, corresponding to the lattice constant of $a = 5.110$ Å and $c = 13.95$ Å. Both of the a- and c-axes lengths were slightly larger in the a-axis oriented film than in the c-axis oriented one.

The lattice constants of our films were somewhat different from those of bulk [$a = 5.1570(4)$ and $c = 13.610(1)$ Å at room temperature].[14,32,33] In our Ti_2O_3 films, a- (c-) axis length contracted (expanded) against the bulk values. Nevertheless, the unit cell volume was almost consistent among the films and bulk. The unit cell volume of trigonal Ti_2O_3 (V_T) was calculated as $V_T = (\sqrt{3}/2)a^2c$. The V_T of the a- and c-axes oriented films and bulk was estimated to be 315.41, 311.22, and 313.46 Å^3, respectively. The difference in V_T was less than $\pm 1\%$ between the films and bulk. However, the c/a ratio characterized lattice deformation: 2.730, 2.703, and 2.639 for a- and c-axes oriented films and bulk at RT, respectively. The Ti_2O_3 films exhibited the larger c/a ratios although the ratios were typical of most of corundum-type oxides. For instance, the c/a ratio of α-Al_2O_3 ($a = 4.759$ Å, $c = 12.991$ Å) is 2.730. The c/a ratio of the a-axis oriented film being identical to that of α-Al_2O_3

implies an interesting mechanism in strained heteroepitaxy on the *a*-plane (both *a*- and *c*-axes are parallel to the interface).

The deviation of lattice constants from bulk values may arise from the competition between the *c*/*a* ratio and unit cell volume in Ti_2O_3 films. Epitaxial strain usually constrains the in-plane lattice, variation of which is compensated along the out-of-plane direction so that the unit cell volume tends to be kept intact.[34] On the other hand, corundum-type Ti_2O_3 has rigid lattice taking quite anisotropic behaviors due to the Ti^{3+}–Ti^{3+} dimer along the *c*-axis. In bulk Ti_2O_3, the *c*/*a* ratio drastically changes from 2.639 (23 °C) to 2.723 (595 °C) mainly due to the elongation of the *c*-axis length (from 13.610 to 13.957 Å).[35] By contrast, the *a*-axis length slightly decreases with temperature (less than 1% reduction from 23 °C to 595 °C) rather against increase in the unit cell volume. In fact, our *a*- and *c*-axes oriented Ti_2O_3 films showed almost the same *a*-axis length (5.110 and 5.104 Å, respectively).

Ti_2O_3 films grown at 1000 °C would have a *c*/*a* ratio close to 2.73, and lattice deformation would take place during the temperature quench. For the *c*-axis oriented film, its *c*-axis length, along out-of-plane free from the substrate constraint, could decrease to reduce the *c*/*a* ratio and unit cell volume. As a result, the *c*/*a* ratio settles a compromised value (2.703) with a unit cell volume smaller than that of the bulk. As for the *a*-axis film having no degree of lattice freedom (both *a*- and *c*-axes are parallel to the interface), the *c*/*a* ratio remains to be 2.73, which is identical to that of α-Al_2O_3 and the unit cell volume becomes larger than that of the bulk.

Formation of corundum-type Ti_2O_3 films was also confirmed from XAS and PES measurements. Figure 2(a) shows Ti 2*p* XAS spectra of *a*- and *c*-axes oriented Ti_2O_3 films before and after Ar-bombardment. Before Ar-bombardment, the Ti 2*p* XAS spectra of the films were similar to the Ti^{4+} reference spectrum owing to oxidation layers at the film surface. Meanwhile, the Ti 2*p* XAS spectra after Ar-bombardment were in good agreement to that of Ti^{3+} (bulk Ti_2O_3), irrespective of film orientation.[36] The Ti L_3 edge still indicates additional structure at 457 eV although our Ar-bombardment process removes the surface layers of more than 10 nm. Considering a few nm of surface oxidation layers [which was estimated from the PES spectra of Fig. 2(b)], the additional structure was attributed to the tetravalent state arising from the slight residual of surface oxidation layers and/or re-oxidized surface layers during XAS and PES measurements. Such additional structure was also found in the Ti 2*p* XAS spectrum of bulk $LaTiO_3$ due to Ti^{4+} impurities.[37]
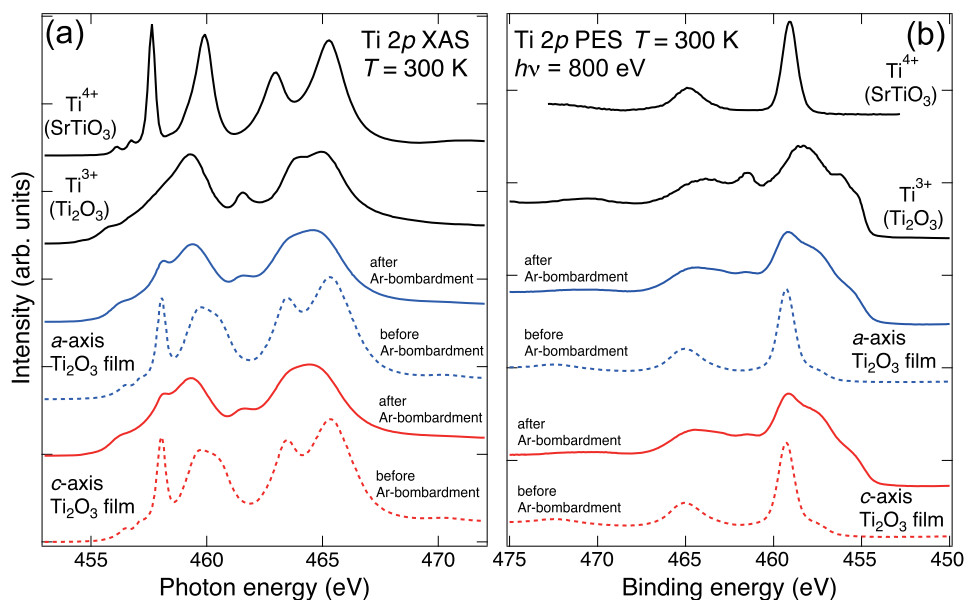

FIG. 2. (a) Ti 2*p* x-ray absorption spectra and (b) Ti 2*p* core-level spectra of *a*- and *c*-axes oriented Ti_2O_3 films. The Ti^{4+}($SrTiO_3$) and Ti^{3+} (bulk Ti_2O_3) spectra taken from Ref. 36 are also plotted as references.

The trivalent states of Ti ions were also confirmed from Ti $2p$ core-level spectra [Fig. 2(b)]. The Ti $2p$ spectral shape of the films after Ar-bombardment exhibited complex structures being similar to the Ti^{3+} reference spectrum (bulk Ti_2O_3).[36] It is described in Ref. 36 that Ti_2O_9 cluster, involving the Ti^{3+}–Ti^{3+} dimer in face-shared TiO_6 octahedral pair, is responsible for the complex spectral features. In fact, Ti $2p$ core-level spectra reported for perovskite titanates of $LnTiO_3$ (where Ln is Lanthanoids) are entirely different from our spectra.[38] These results verify the electronic states of corundum-type Ti_2O_3. We note that a trace of tetravalent states, such as the additional structure centered at 459 eV, was also seen in the core-level spectra. In fact, the Ti $2p$ core-level spectra of the films before Ar-bombardment show almost the same spectral shape of the Ti^{4+} reference spectrum. The small components attributed to Ti^{3+} states were also found around ∼457 eV. Taking the penetration depth of photoelectrons of ∼1 nm into account, the thickness of the surface oxidation layers is expected to be a few nm.

Figure 3 shows temperature dependence of resistivity (ρ) for Ti_2O_3 films. The bulk Ti_2O_3 data taken from Ref. 19 are also plotted for comparison.[19] In bulk Ti_2O_3, the IMT occurs around 450 K.[14–19] In the following discussion, we describe the electric properties of Ti_2O_3 films based on the ρ-T data of bulk Ti_2O_3. We assume that our Ti_2O_3 films are in metallic and insulating states in the high and low temperature limits, respectively, and exhibit one IMT in certain temperature. The c-axis oriented film indicated $\rho \sim 1 \times 10^{-1}$ Ω cm at $T = 2$ K, which first gradually decreased and dropped from ∼200 K to reach ∼3×10^{-4} Ω cm at ∼400 K, suggesting an electronic phase transition. Although the transition-temperature range is much lower for our c-axis oriented film, the observed transition is assignable to an IMT. In fact, no other transitions were found up to 650 K.

The ρ-T curves for the a-axis oriented film are also shown in Fig. 3. The anisotropy in electronic property was investigated along the [0001] (I//c) and [1$\bar{1}$00] ($I \perp c$) directions using the identical films. The resistivity taken along I//c was substantially higher than that along $I \perp c$. For the latter, ρ was ∼5×10^{-1} Ω cm at $T = 2$ K and after the initial drop, it kept a nearly identical value to that of the c-axis oriented film (also measured along $I \perp c$). Above 300 K, the resistivity was higher by about an order of magnitude than that of the c-axis oriented film.

The resistivity taken along I//c was as high as ∼1×10^{3} Ω cm at $T = 2$ K, which was much higher by three orders of magnitude than $I \perp c$. It gradually decreased with increasing temperature and became ∼1 Ω cm at 450 K, while keeping the large difference in resistivity by three orders of magnitude. A broad IMT was clearly observed between 450 K and 600 K for the a-axis oriented film taken along I//c. Because the phase transition was independent of the measurement direction, the IMT also occurred between 450 K and 600 K for the a-axis oriented film taken along $I \perp c$. After

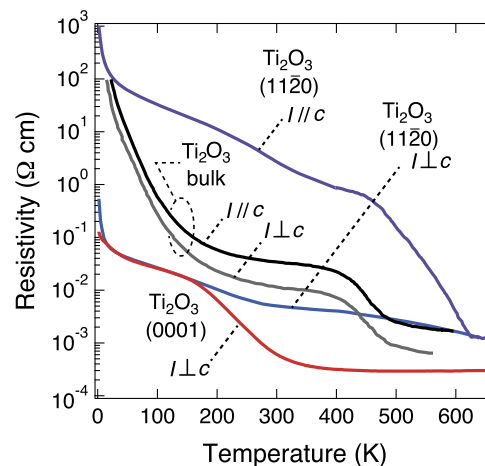FIG. 3. Temperature dependence of resistivity for Ti_2O_3 films. The blue and purple lines indicate the a-axis Ti_2O_3 films measured along $I \perp c$ and I//c directions, respectively. The red line indicates the c-axis Ti_2O_3 films. The bulk Ti_2O_3 data taken from Ref. 19 are also shown for comparison. The black and gray lines indicate the measurement directions along I//c and $I \perp c$, respectively.

the transition, the resistivity was independent of the measurement directions. As for bulk Ti_2O_3, the transition starts to occur at ~400 K accompanying a smaller resistivity drop.[14–19] The IMT as well as anisotropy in resistivity is largely enhanced in our *a*-axis oriented Ti_2O_3 films: the higher transition temperature and the larger resistivity change. It is noteworthy that the ρ-T curve taken along $I//c$ asymptotically approaches bulk values at both low and high temperature limits. This fact implies that the insulating and metallic ground states in our film are identical to those in the bulk.

In order to investigate the origin of enhanced anisotropy in further detail, we took or performed Hall-effect measurements at various temperatures (Fig. 4). Figure 4(a) shows temperature dependence of the inverse Hall coefficient ($1/R_H$) for Ti_2O_3 films. The Hall coefficients indicated positive signs for all the Ti_2O_3 films, which was in agreement with bulk Ti_2O_3,[16,39] suggesting that majority charge carriers were holes. The $1/R_H$ values were ~10 C/cm^3 at 10 K and ~100 C/cm^3 at 300 K regardless of the film orientation and measurement direction, while higher than that in bulk by about an order of magnitude.[16] The data in Fig. 4(a) can be seen against the right-hand scale to estimate charge carrier density ($1/R_H e$) ranging from 10^{20} to 10^{21} cm^{-3}, which are smaller than one carrier per Ti site (3.8×10^{22} cm^{-3}). Hall mobility R_H/ρ plotted in Fig. 4(b) was as high as 1–10 cm^2/V s along $I \perp c$, which was comparable to that of bulk Ti_2O_3.[16] By contrast, Hall mobility along $I//c$ was 10^{-3} cm^2/V s, which was smaller by three orders of magnitude than that along $I \perp c$. These results indicate that the enhanced anisotropy originates from substantial difference in the mobility.

The modulation of the IMT induced by the film orientation is also reported in VO_2, that is, the identical d^1 electron configuration to Ti_2O_3.[20–28] Li and Dho reported on the IMT of VO_2 films grown on TiO_2 substrates with five different orientations. The T_{IMT} varied from 310 K [(110) orientation] to 350 K [(001) orientation], while keeping the resistivity change by 3–4 orders of magnitude across the IMT.[27] In VO_2 films, T_{IMT} is known to depend on the *c*-axis length. The shorter *c*-axis length is, the lower T_{MIT} becomes. This is because the shorter *c*-axis length (V^{4+}–V^{4+} distance) increased *d*-bandwidth and stabilized the metallic rutile phase.[24–26] The relationship between the *c*-axis length and T_{IMT} in VO_2 is completely opposite to bulk Ti_2O_3. In addition, the IMT in VO_2 accompanying the structural phase transition (orthorhombic to rutile) is in striking contrast to that in Ti_2O_3 because the corundum-type structure is maintained in the whole temperature range. The difference in structural
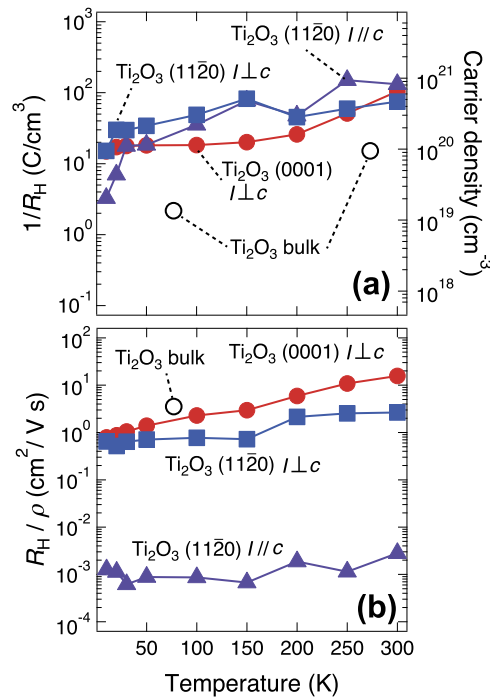

FIG. 4. Temperature dependence of (a) $1/R_H$ and (b) R_H/ρ of Ti_2O_3 films. The marker colors correspond to those in Fig. 3. The data of bulk Ti_2O_3 are also shown as Ref. 16.

transition also influences the width of transition temperature between Ti_2O_3 and VO_2. As shown in Fig. 3, Ti_2O_3 showed the gradual resistivity change in a range of ~100 °C owing to the lattice deformation without the structural phase transition. By contrast, VO_2 showed the sharp IMT depending on the domain size with the temperature width of ~10 K accompanying the structural phase transition.[28]

In Ti_2O_3, the simple IMT model was proposed by Van Zandt *et al.*[40] In the model, the *c/a* ratio governs the degree of splitting in the t_{2g} levels and is responsible for the IMT. Owing to the smaller *c/a* ratio, the Ti–Ti pairs are formed along the [0001] direction across the trigonal distorted TiO_6 octahedra, and the non-degenerate a_{1g} orbital lies in the lowest energy level in Ti 3*d* orbitals. The hybridization of two a_{1g} orbitals along the [0001] direction forms bonding (a_{1g}) and anti-bonding (a_{1g}^*) levels. The degenerate e_g^π orbitals create $e_g^\pi + e_g^{\pi^*}$ levels between the a_{1g} and a_{1g}^* ones. The Ti 3*d* electrons occupy only in the a_{1g} levels, resulting in electron-localized insulating states.[41] According to the previous temperature dependence of structural analysis of pure Ti_2O_3 bulk, the *c/a* ratio increases with increase in temperature and it reaches 2.7 at 600 K, where metallic phase completely appears.[33,35] Meanwhile, although our *a*-axis oriented Ti_2O_3 film exhibited the *c/a* ratio of 2.73 even at room temperature, the film still showed the insulating behavior (Fig. 3). These results suggest that the simple IMT model cannot be applied to Ti_2O_3 films.

Instead of the simple IMT model, another IMT mechanism of change in 3*d* orbital occupation was recently proposed by Tanaka.[36,42,43] It is described in Ref. 40 that Ti 3*d* electrons dominantly occupies in $d_{3z^2-r^2}$ orbitals that expand perpendicular to the *c*-plane in the insulating phase. Assuming that the film surface strongly affects the electronic structures in Ti_2O_3, the film orientation can control T_{IMT}. The $d_{3z^2-r^2}$ orbitals are elongated parallel and perpendicular to the film surface for *a*- and *c*-axes oriented films, respectively. Taking the unstable orbitals perpendicular to the film at the surface into account, the occupation of the $d_{3z^2-r^2}$ orbitals would become smaller for the *c*-axis oriented films, leading the unstable insulating phase. To reveal difference in orbital occupation according to the film orientation, X-ray linear dichroism measurements to our films will be required.[36]

Finally, we would like to emphasize that the Ti_2O_3 film is a useful Mottronics material like VO_2. VO_2 exhibits a large resistivity drop by more than three orders of magnitude across the IMT,[20–28] which was also found for our *a*-axis oriented Ti_2O_3 film taken along the *I//c* direction. The experimental fact that resistivity change across the IMT strongly depends on the direction suggests that the Ti_2O_3 based devices must align along the specific crystal axis. In addition, our *a*-axis oriented Ti_2O_3 film is superior to the VO_2 film in terms of thermal stability in Mottronics devices owing to higher T_{IMT} far above room temperature. To utilize it for active devices, appearance of the carrier-doping induced IMT is indispensable. In bulk Ti_2O_3, substitution of the Ti site by V, which corresponds to hole doping, suppresses the insulating phase, resulting in metallic ground states.[19,32,33] Further investigation on substitutional V doping to Ti_2O_3 in the thin-film form is required for future device applications. This fact suggests that field-effect doping using an electric double-layer transistor[20–23] can modulate the electronic phase of Ti_2O_3 thin films at room temperature.

In summary, we have grown *a*- and *c*-axes oriented Ti_2O_3 films by using pulsed-laser deposition and investigated their crystal structures and electronic properties. High-quality and single-crystalline Ti_2O_3 films were obtained on the isostructural α-Al_2O_3 substrates. XAS and PES spectra also confirmed the formation of corundum-type Ti_2O_3 films. The behaviors of temperature dependence of resistivity indicated striking difference in the orientation of the films and the direction of the current path. T_{IMT} was lower (higher) in the *c*-axis (*a*-axis) oriented films than that in the bulk. The large resistivity drop by three orders of magnitude was observed along *I//c* rather than $I \perp c$. The large anisotropy in conductivity was attributed to a difference in Hall mobility, parallel or perpendicular to the *c*-axis direction. Ti_2O_3 films with higher T_{IMT} and large change in resistivity across IMT unveil their useful characteristics toward the Mottronics application.

[1] A. Fujishima and K. Honda, Nature **238**, 37 (1972).

[2] A. Fujishima, X. Zhang, and D. A. Tryk, Surf. Sci. Rep. **63**, 515 (2008).

[3] Y. Furubayashi, T. Hitosugi, Y. Yamamoto, K. Inaba, G. Kinoda, Y. Hirose, T. Shimada, and T. Hasegawa, Appl. Phys. Lett. **86**, 252101 (2005).

[4] N. J. Doyle, J. K. Hulm, C. K. Jones, R. C. Miller, and A. Taylor, Phys. Lett. A **26**, 604 (1968).

[5] J. K. Hulm, C. K. Jones, R. A. Hein, and J. W. Gibson, J. Low Temp. Phys. **7**, 291 (1972).

[6] S. Lakkis, C. Schlenker, B. K. Chakraverty, R. Buder, and M. Marezio, Phys. Rev. B **14**, 1429 (1976).

[7] T. Tonogai, H. Takagi, C. Murayama, and N. Mori, Rev. High Pressure Sci. Technol. **7**, 453 (1998).

[8] H. Ueda, K. Kitazawa, H. Takagi, and T. Matsumoto, J. Phys. Soc. Jpn. **71**, 1506 (2002).

[9] L. J. D. Jongh, Physica C **152**, 171 (1988).

[10] R. Micnas, J. Ranninger, and S. Robaszkiewicz, Rev. Mod. Phys. **62**, 113 (1990).

[11] C. Zhang, F. Hao, G. Gao, X. Liu, C. Ma, Y. Lin, Y. Yin, and X. Li, npj Quantum Mater. **2**, 2 (2017).

[12] Y. Li, Y. Weng, J. Zhang, J. Ding, Y. Zhu, Q. Wang, Y. Yang, Y. Cheng, Q. Zhang, P. Li, J. Lin, W. Chen, Y. Han, X. Zhang, L. Chen, X. Chen, J. Chen, S. Dong, X. Chen, and T. Wu, NPG Asia Mater. **10**, 522 (2018).

[13] K. Yoshimatsu, O. Sakata, and A. Ohtomo, Sci. Rep. **7**, 12544 (2017).

[14] C. N. R. Rao, R. E. Loehman, and J. M. Honig, Phys. Lett. A **27**, 271 (1968).

[15] F. J. Morin, Phys. Rev. Lett. **3**, 34 (1959).

[16] J. M. Honig and T. B. Reed, Phys. Rev. **174**, 1020 (1968).

[17] J. M. Honig, Rev. Mod. Phys. **40**, 748 (1968).

[18] G. V. Chandrashekhar, Q. W. Choi, J. Moyo, and J. M. Honig, Mater. Res. Bull. **5**, 999 (1970).

[19] M. Uchida, J. Fujioka, Y. Onose, and Y. Tokura, Phys. Rev. Lett. **101**, 066406 (2008).

[20] M. Nakano, K. Shibuya, D. Okuyama, T. Hatano, S. Ono, M. Kawasaki, Y. Iwasa, and Y. Tokura, Nature **487**, 459 (2012).

[21] J. Jeong, N. Aetukuri, T. Graf, T. D. Schladt, M. G. Samant, and S. S. P. Parkin, Science **339**, 1402 (2013).

[22] K. Shibuya and A. Sawa, Adv. Electron. Mater. **2**, 1500131 (2016).

[23] T. Kanki and H. Tanaka, APL Mater. **5**, 042303 (2017).

[24] Y. Muraoka and Z. Hiroi, Appl. Phys. Lett. **80**, 583 (2002).

[25] K. Nagashima, T. Yanagida, H. Tanaka, and T. Kawai, J. Appl. Phys. **100**, 063714 (2006).

[26] K. Nagashima, T. Yanagida, H. Tanaka, and T. Kawai, J. Appl. Phys. **101**, 026103 (2007).

[27] J. Li and J. Dho, J. Cryst. Growth **404**, 84 (2014).

[28] H. Takami, K. Kawatani, H. Ueda, K. Fujiwara, T. Kanki, and H. Tanaka, Appl. Phys. Lett. **101**, 263111 (2012).

[29] H. Kurokawa, K. Yoshimatsu, O. Sakata, and A. Ohtomo, J. Appl. Phys. **122**, 055302 (2017).

[30] A. Radetinac, K. S. Takahashi, L. Alff, M. Kawasaki, and Y. Tokura, Appl. Phys. Express **3**, 073003 (2010).

[31] I. Sunagawa, K. Narita, P. Bennema, and B. Van Der Hoek, J. Cryst. Growth **42**, 121 (1977).

[32] J. J. Capponi, M. Marezio, J. Dumas, and C. Schlenker, Solid State Commun. **20**, 893 (1976).

[33] C. E. Rice and W. R. Robinson, J. Solid State Chem. **21**, 145 (1977).

[34] C. Adamo, X. Ke, H. Q. Wang, H. L. Xin, T. Heeg, M. E. Hawley, W. Zander, J. Schubert, P. Schiffer, D. A. Muller, L. Maritato, and D. G. Schlom, Appl. Phys. Lett. **95**, 112504 (2009).

[35] C. E. Rice and W. R. Robinson, Acta Crystallogr., Sect. B: Struct. Crystallogr. Cryst. Chem. **33**, 1342 (1977).

[36] C. F. Chang, T. C. Koethe, Z. Hu, J. Weinen, S. Agrestini, L. Zhao, J. Gegner, H. Ott, G. Panaccione, H. Wu, M. W. Haverkort, H. Roth, A. C. Komarek, F. Offi, G. Monaco, Y. –F. Liao, K. –D. Tsuei, H. –J. Lin, C. T. Chen, A. Tanaka, and L. H. Tjeng, Phys. Rev. X **8**, 021004 (2018).

[37] M. Abbate, F. M. F. de Groot, J. C. Fuggle, A. Fujimori, Y. Tokura, Y. Fujishima, O. Strebel, M. Domke, G. Kaindl, J. van Elp, B. T. Thole, G. A. Sawatzky, M. Sacchi, and N. Tsuda, Phys. Rev. B **44**, 5419 (1991).

[38] K. Morikawa, T. Mizokawa, A. Fujimori, Y. Taguchi, and Y. Tokura, Phys. Rev. B **54**, 8446 (1996).

[39] J. Yahia and H. P. R. Frederikse, Phys. Rev. **123**, 1257 (1961).

[40] L. L. Van Zandt, J. M. Honig, and J. B. Goodenough, J. Appl. Phys. **39**, 594 (1968).

[41] H. J. Zeiger, Phys. Rev. B **11**, 5132 (1975).

[42] A. Tanaka, J. Phys. Soc. Jpn. **73**, 152 (2004).

[43] H. Sato, A. Tanaka, M. Sawada, F. Iga, K. Tsuji, M. Tsubota, M. Takemura, K. Yaji, M. Nagira, A. Kimura, T. Takabatake, H. Namatame, and M. Taniguchi, J. Phys. Soc. Jpn. **75**, 053702 (2006).